Appl Phys A (2012) 106:257–263
DOI 10.1007/s00339-011-6691-7

Applied Physics A
Materials Science & Processing

INVITED PAPER

Nonlinear imaging and THz diagnostic tools in the service of Cultural Heritage

G. Filippidis · M. Massaouti · A. Selimis · E.J. Gualda · J.-M. Manceau · S. Tzortzakis

Received: 7 July 2011 / Accepted: 7 November 2011 / Published online: 19 November 2011

Abstract We present the use of novel nonlinear imaging, terahertz time-domain spectroscopy and imaging as powerful diagnostic tools for studies of works of art. It is shown that nonlinear imaging offers precise in-depth information, while terahertz imaging can reveal hidden objects and uncover information on highly absorbing organic compounds whose visualization is difficult in other parts of the spectrum.

1 Introduction

The removal of unwanted surface layers consists one of the most delicate interventions in Cultural Heritage (CH) conservation. In particular, both time and exposure to atmospheric conditions may irreversibly modify these layers, calling thus for their removal. However, either by conventional cleaning methods or lately by laser beam application, the conservator interacts directly and irreparably with the cultural material. The removal action gets further complicated if the plurality of materials that may be found within a painted artwork (often in ultrathin layers or traces) is taken into account. Therefore, given the demanded high selectivity and special treatment, a detailed in-depth assessment of the painting layers compounds is required. A variety of techniques has been employed towards the analysis and characterization of materials spanning from X-rays up to the mid-infrared.

In the present study, two femtosecond laser-based novel approaches are described: nonlinear imaging and terahertz (THz) time-domain spectroscopy and imaging. The former relying on nonlinear phenomena taking place upon intense laser irradiation, including Multi-Photon Excitation Fluorescence (MPEF), Second Harmonic Generation (SHG) and Third Harmonic Generation (THG), while the latter is based on the use of femtosecond laser induced Terahertz radiation.

Both of the presented herein techniques are non-invasive and can reliably and accurately reveal in-depth information (e.g. structural modifications and hidden objects below the original surface) of a cultural object layers leading to the mapping of the artwork to be restored. We anticipate that they can serve as monitoring tools to fine-tune the cleaning protocol and safeguard the CH object.

2 Nonlinear imaging: principles and applications

MPEF, SHG and THG, are well-established, non-destructive imaging techniques that recently have been used as diagnostic tools for art conservation studies, providing very promising results [1, 2]. They have the potential to provide essential information to the art conservation scientists for the assessment of the appropriate conservation method that has to be followed for a painted artwork [3].

The use of femtosecond (fs) lasers enables high peak powers for efficient nonlinear excitation, but at low enough energies so that samples are not damaged. The basic principle underlying MPEF, SHG and THG imaging techniques is that for tightly focused fs laser pulses, the photon density is high enough to induce multiphoton absorption or

G. Filippidis (✉) · M. Massaouti · A. Selimis · E.J. Gualda · J.-M. Manceau · S. Tzortzakis
Institute of Electronic Structure and Laser, Foundation for Research and Technology Hellas, P.O. Box 1527, 71110, Heraklion, Greece
e-mail: filip@iesl.forth.gr

S. Tzortzakis
e-mail: stzortz@iesl.forth.gr
url: http://unis.iesl.forth.gr

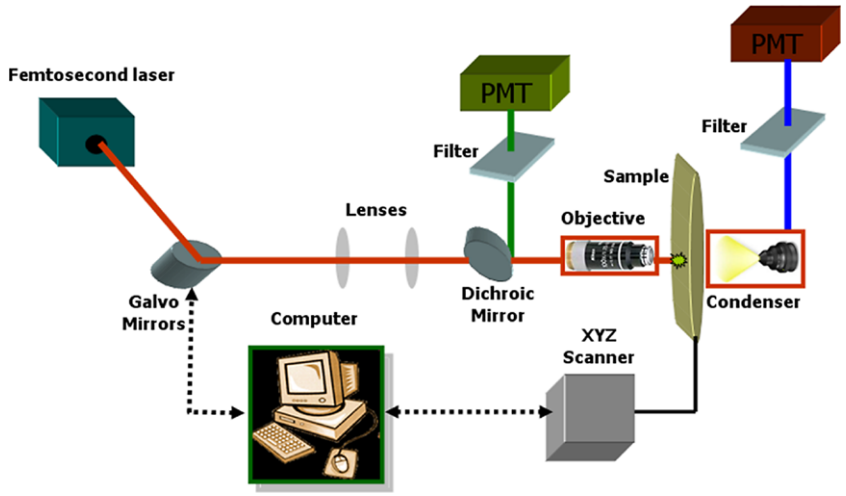

Fig. 1 Schematic of the nonlinear imaging experimental setup with two pathways of detection one in the reflection and the other in the transmission mode. PMT is photomultiplier tube

other nonlinear, coherent processes within the focal volume. Nonlinear imaging modalities present the capability of intrinsic three-dimensionality (3-D), high axial resolution and the ability to section deep within the sample. Out of focal plane photobleaching and phototoxicity phenomena are dramatically reduced, diminishing damage of the studied object. For SHG and THG (scattering coherent processes) an additional advantage derives from the fact that no energy is deposited on specimens, thus sample disturbance (e.g., thermal, mechanical side-effects) are minimal, which is desirable for art conservation studies. MPEF imaging measurements (Two or Three Photon Excitation Fluorescence (2PEF/3PEF)) provide information related to the identification of the chemical composition of artifacts. On the other hand, SHG signal is produced from non-centrosymmetric molecules. SHG modality provides information related to structures with high degree of orientation and organization but without inversion symmetry such as stacked membranes and arranged proteins (e.g. collagen) [4]. THG is sensitive to local differences in third-order nonlinear susceptibility $\chi^{(3)}$, refractive index and dispersion [5, 6]. Under tight focusing conditions, the extent of the THG signal increases dramatically when the beam focus spans an interface between two optically different materials. This allows imaging based on THG to resolve otherwise transparent interfaces and inhomogeneities within the resolution of the confocal parameter and without the use of external dyes. No THG signal is collected when the laser beam is focused inside a homogeneous, normally dispersive medium. Consequently, THG comprises an ideal diagnostic tool that gives unique structural and morphological information for various samples. In contrast to SHG modality that requires a medium without inversion symmetry, THG is allowed in any medium.

Multiphoton excitation microscopy measurements have been used to recover lost information in the area of archaeology [7]. Additionally, SHG imaging measurements have been applied for the evaluation of corrosion of painted metals [8]. Recently, higher harmonic generation (SHG-THG) spot measurements were implemented for the extraction of information related to thickness determination and composition discrimination of various types of natural and synthetic glue used for lining of painted artworks [9]. Nonlinear imaging modalities were employed for the precise and non-destructive thickness detection and composition identification of complex, multilayer structures used in model painted artworks. Specifically, via the detection of THG and MPEF signals from model painted artworks, the precise thickness determination of varnish protective layers and the identification of the chemical composition of the artifacts were achieved [1, 2]. Detection takes place in both transmission and reflection mode, demonstrating the ability to apply this non-destructive technique on the evaluation of original artworks [2].

2.1 Nonlinear microscopy setup

The nonlinear signals (MPEF, SHG and THG) are generated simultaneously from the focal volume at the sample plane. The development of an experimental apparatus that allows the collection of different nonlinear optical signals simultaneously (in the reflection and in the transmission mode) in order to obtain complementary information from the samples is depicted in Fig. 1 and is described in detail in previous reports [1]. Briefly, the system consists of an Amplitude Systems femtosecond laser operating at 1028 nm, with average power of 1 Watt, delivering 200 fs pulses at a repetition rate of 50 MHz. Since the third harmonic of the laser system is in the near ultraviolet (UV) region of the electromagnetic spectrum (∼343 nm), there is no need to use UV optics with special coatings for the collection of the THG signal. The focal plane is selected with the motorized translation stage (1 μm resolution). In order to get high resolution images,

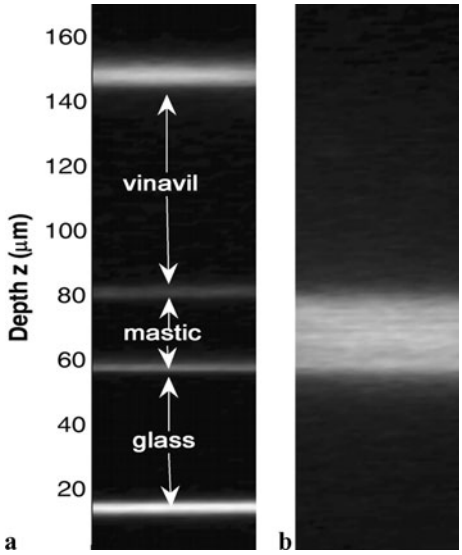

Fig. 2 Precise sectioning of a multilayer sample ((**a**) THG and (**b**) 3PEF) containing a layer of vinavil and a layer of mastic. The lateral dimension of the scanning area of the recorded images is 15 μm

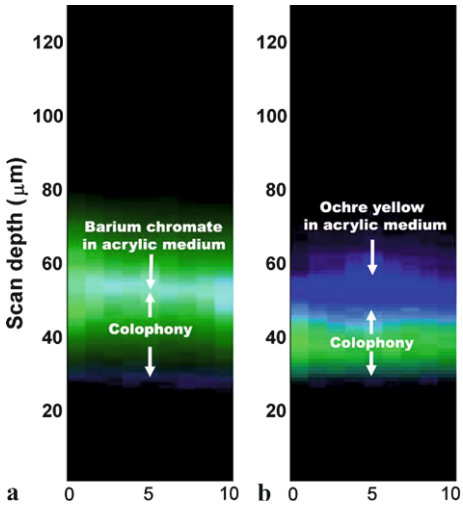

Fig. 3 Sections of samples with a layer of colophony and a layer of pigment: (**a**) barium chromate in acrylic medium and (**b**) *ochre yellow* in acrylic medium. *Blue* represents THG and *green* MPEF signals. The lateral dimension of the scanning area of the recorded images is 10 μm. Detection took place in the reflection mode

the scanning is performed by a pair of galvanometric mirrors. Lab View interface used to control both scanning and data acquisition procedures. MPEF signals are collected in the backward direction using a photomultiplier tube (PMT) connected to a Lock in Amplifier ensuring thus high signal-to-noise ratio. THG signals are detected simultaneously in the forward direction, by employing a second PMT and a Lock in Amplifier. Additionally, the detection of THG signals in the reflection mode is feasible. In this case THG and MPEF signals are collected in distinct set of measurements.

This experimental setup (with two pathways of detection) has been employed for carrying out nonlinear imaging measurements in model painting samples: a multilayer varnish sample and artifacts simulating real case artworks.

2.2 Multilayer varnish sample

Figure 2 shows a sample combining layers of vinavil and mastic varnishes of different thickness. The sample was placed on a glass plate. Through THG measurements (Fig. 2(a)) four different layers can be distinguished indicating the interface between the different media. The upper one corresponds to the air/vinavil interface and the lower one to the glass/air interface. The other two represent the vinavil/mastic and mastic/glass interfaces, respectively. The precise sectioning of the multilayer sample can be achieved (measured thickness of the vinavil layer ∼63 μm, thickness of the mastic layer ∼22 μm). The axial resolution is of the order of 2 microns. The energy per pulse on the sample is less than 1 nJ. The MPEF signals from the sample are depicted in Fig. 2(b). It can be observed that signals only arise from the layer of mastic, providing complementary information for the multilayer sample. These measurements would be extremely helpful in a variety of applications, such as the identification of new and old varnish layers of complex multilayer structures and the recognition of polymerized or oxidized varnish and more generally organic layers.

2.3 Model painted artifacts

Figure 3, presents the two dimensional section of two model samples. These simulations of real artworks were composed with ready-made acrylic paint (Rowney CRYLA, artistic acrylic color) as binding medium and different kinds of pigment. Sample 1 (Fig. 3(a)) is lemon yellow ($BaCrO_4$) and sample 2 (Fig. 3(b)) is an ochre yellow ($Fe_2O_3{*}nH_2O$, SiO_2, Al_2O_3) pigment. Both model samples were covered with the same natural varnish protective material (colophony). Combining THG (blue) and MPEF (green) signals are depicted in Fig. 3. It should be pointed out that both nonlinear signals are detected in the reflection mode.

The two first interfaces, between different media, are detectable via THG imaging measurements (blue). From the reflected THG signal, the air/colophony and the colophony/pigments interfaces can be distinguished for the two samples. The precise determination of the thicknesses of the protective varnish layers in the two model painting materials (24 μm for sample 1 and 21 μm for sample 2) can be achieved. There is a difference between the THG signal obtained from the two interfaces: while the former (air/colophony) is a continuous line, since colophony varnish is a uniform material, the latter (colophony/pigment) is not homogeneous and is only created at the pigments particles. Furthermore, the refractive index mismatch is higher between ochre yellow and colophony interface compared to

respective one of the barium chromate [10]. Consequently, keeping the same illuminating conditions, the efficiency of the THG process is higher for ochre yellow colophony interface (sample 2) than that for barium chromate colophony interface (sample 1). That comprises a possible explanation why the second interface is more clearly distinguished in Fig. 3(b) than in Fig. 3(a). Moreover, the different absorption of the THG signal from the various pigment layers must be taken into account.

MPEF signals (green) present almost the same level of intensity for the varnish and for the pigmented material for sample 1 (Fig. 3(a)). On the contrary, the recorded MPEF signal for sample 2 (Fig. 3(b)) arises only from the colophony varnish. The pigmented material of sample 2 is not generating any MPEF signal. Therefore, MPEF measurements can provide complementary information that allows the discrimination, rather than the determination, of the composites of different painting media.

Nonlinear image contrast modalities (MPEF, SHG, THG) comprise a powerful diagnostic tool for art conservation studies facilitating the control of any cleaning interventions. The combination of these modalities with other non-invasive techniques such as Confocal Raman Microscopy can give additional information for the analysis of different layers and the identification of materials as a function of depth [11].

We have to note that the compact size of the employed excitation femtosecond sources and the reduced time of data acquisition make this innovative technique ideal for in-situ laser diagnosis of painted artworks.

3 Terahertz imaging and spectroscopy

As is mentioned above, up to date, several scientific techniques are used in order to analyze and identify the materials found in artworks (such as pigments, natural varnishes, synthetic coatings and dyes, etc.), including also those used in previous "interventions". Such studies are essential since in comparison to historic references facilitate art historians to draw conclusions about the period that the artwork was created and the artists' technique and thus potentially verify the authenticity of an artwork. In addition, through spectral imaging, significant information on the preservation state and previous interventions of the artwork can be drawn which will assist conservators to decide on the necessary conservation strategies.

Although there are many well-established techniques [12–15], like mid-infrared, Raman spectroscopy and X-Rays fluorescence which have been successfully used for identifying organic and inorganic materials of art interest, in the past few years, a rapidly increasing interest is noticed in terahertz (THz) spectroscopy and imaging and their implementation to CH studies [16–20]. THz radiation lies in the far-infrared region of the electromagnetic spectrum ranging from 0.1 to 10 THz (3.3–333 cm^{-1}) and in contrast to X-rays, it constitutes a non-ionizing radiation (1 THz = 4.43 meV). Thus it poses no health risk or radiation damage to the object under study. The THz spectrum provides rich information of low frequency vibrational modes such as crystalline lattice or intermolecular vibrational modes, hydrogen bonding stretches, and large-scale motions of an entire macromolecule. In other words, it is the structure of the molecules, constituting the material, which determines the THz spectrum. Unlike mid- and near-infrared spectroscopy that observes the intramolecular behavior, THz spectroscopy can discriminate the different materials mixed in a paint, complementing the rather complicated IR spectra.

One of the biggest advantages of THz is that, as submillimeter waves, they can penetrate through a wide variety of materials such as paper, wood, masonry, clothing, plastic and ceramics, which are usually opaque to both visible and infrared radiation. In comparison to X-rays and microwaves which can penetrate thick layers and are often used to reveal hidden underdrawings below the painting layers of an artwork, find dislocations, water damages and other defects, THz exhibit better depth and lateral spatial resolution [21, 22]. These transmission properties of the THz radiation in combination with the fact that information can simultaneously be obtained for the internal structure of an artwork, without requiring any sample specimen, point out the potential of THz waves to become an essential tool for art analysis in the near future.

3.1 The terahertz-time domain spectroscopy (THz-TDS) system

Nowadays, numerous techniques including photoconductive antennas [23] and optical rectification [24] are widely used for the generation of THz pulses. However, these techniques have some important drawbacks related to the low power of the source, the very narrow spectra of the pulses, as well as the lack of tunability of the source. Here we employ a different approach based on the photo-ionization of gases using intense femtosecond pulses and laser filaments that addresses all the above mentioned drawbacks.

In this approach, the THz emission is the result of a transversal plasma photocurrent produced from a synthesized 2-color (ω and 2ω) asymmetric laser field [25]. One direct advantage of this technique is that controlling the phase between the ω and 2ω laser fields one gains control on the polarization of the THz field and for this different possibilities have been proposed, via the positioning of the frequency doubling crystal [26], or through the use of an attosecond phase controller [27] and via the accurate control of the surrounding gas pressure [28]. Moreover using

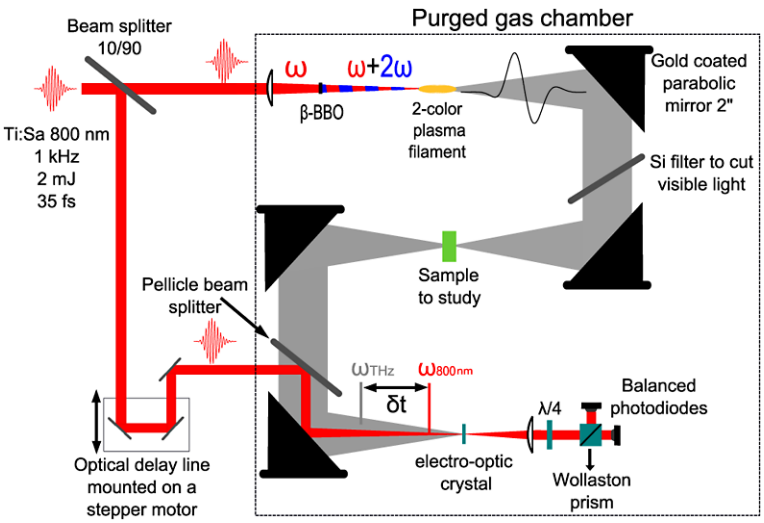

Fig. 4 Schematic representation of the THz-TDS experimental setup

filamentation tailoring techniques we have demonstrated the ability to control the THz electric field shape, and thus, its spectrum [29] as well as the intensity of the source [30].

Our THz-TDS system is based on a pump-probe, coherent detection approach and is shown in Fig. 4. A powerful amplified kHz Ti:Sa laser system delivering 35 fs pulses at 800 nm central wavelength and energy of 1.45 mJ per pulse is used. The initial beam is split in two arms (10% and 90%, respectively). The most intense one, with energy equal to 1.3 mJ and a Gaussian beam profile with a diameter of 6.6 mm, is focused in ambient air with a positive lens ($f = +200$ mm) and partially doubled in frequency in a BBO crystal (50 μm thick) to produce a 2-color filament and subsequently THz radiation. A ratio of 1/9 between the fundamental and the second harmonic laser fields has been indentified to be the optimum, above and below which the strength of the emitted THz field is considerably lower. The second arm, after being further attenuated, is used for probing the THz-induced birefringence in an electro-optic crystal and monitoring the time profile of the THz electric field. This coherent detection technique is known as electro-optic sampling [31]. A balanced detection is used to measure the induced phase delay on the probe beam. For the collection, collimation and refocusing the generated THz beam to the detection crystal, a set of four parabolic mirrors is used, as depicted in Fig. 4. A high resistivity silicon wafer (1 mm thick) placed at Brewster's angle just after the first parabolic mirror, insures that the residual laser beam is blocked from the THz beam path. Finally, the whole setup is enclosed in a purged gas (e.g. N_2) chamber for eliminating THz absorption from water vapor.

3.2 THz imaging

The THz system we described above can be used for imaging purposes by recording transmission or reflection THz

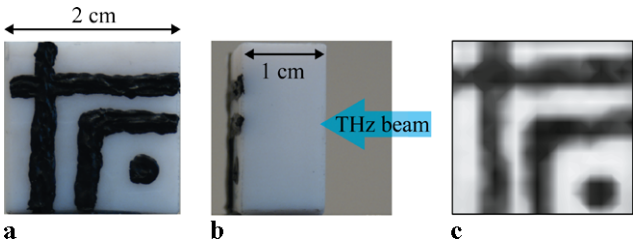

Fig. 5 THz imaging. (**a**) Photo of the black drawing (Mars Black Acrylic) (**b**) Side view of the sample and direction of the THz radiation, (**c**) the THz recomposed image of the drawing

spectra of the sample under study at different positions (e.g. raster scanning the sample). In this work we demonstrate a THz image as obtained by recording the transmission spectra of the THz pulse through a one sided painted Teflon sample (20×20 mm^2). The sample thickness is 10 mm and its painted side, illustrating a simple Mars Black Acrylic paint drawing, of 300–400 μm thick, is placed on the opposite direction of the THz beam propagation in our THz-TDS system. The raster scanning of the sample is achieved by the aid of a computer controlled x–y translation stage and for each pixel, the full THz electric field transient is recorded. The reconstructed THz image of the drawing presented in Fig. 5c, is the result of the integrated Fourier transformed (FFT) amplitude of the transmitted THz electric field spectra normalized to the initial amplitude of the THz electric field, in the spectral range between 0.4 THz and 2.7 THz. The image consists of 20×20 pixels with 1 mm spacing and for each pixel, it takes about 30 s in order to measure the transmitted THz electric field. Consequently, the full record of the THz image lasts few hours but it could be essentially reduced by using a fast delay line. The lateral resolution is limited by the radiation wavelength and in our case is estimated at about 0.5 mm. The resulting THz image demonstrates the capability of our THz-TDS system to recognize successfully

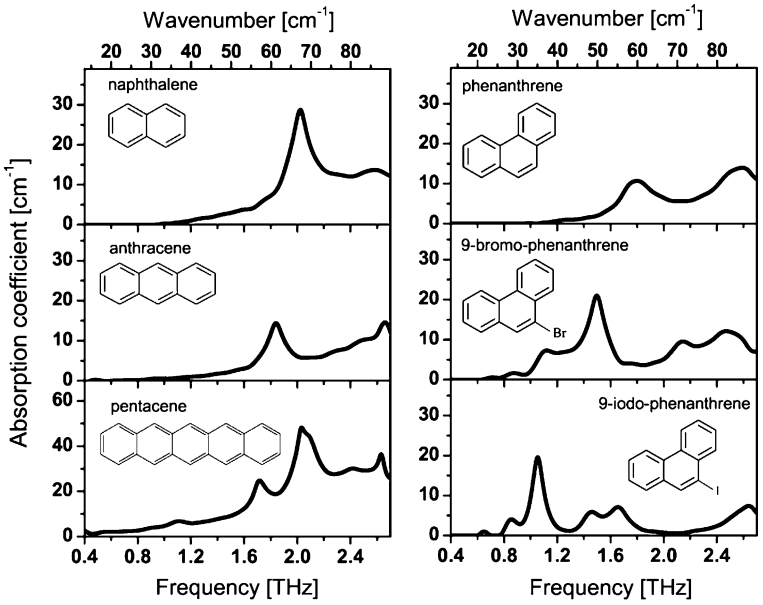

Fig. 6 Absorption spectra of small polycyclic aromatic hydrocarbons and their halogenated compounds in the region between 0.4 THz up to 2.7 THz

a model painting from the back side of on a thick Teflon substrate which would be difficult to obtain with other imaging techniques.

3.3 THz spectroscopy for molecular identification

Beyond the imaging capabilities, this powerful THz-TDS system is used for detecting and rapidly discriminating the molecular structure of highly absorbing, across the electromagnetic spectrum, organic compounds. In this work we present our studies on polycyclic aromatic hydrocarbons (PAHs: such as naphthalene, anthracene, phenanthrene, pentacene, as well as some of their halogenated compounds). Naphthalene and anthracene are two of the five basic raw materials used for the fabrication of coal tar dyes. Upon replacement of one or more of their peripheral hydrogen atoms with some other chemical groups, for example an amino acid ($–NH_2$) or an alcohol (–OH) group, a great number of intermediates (such as aniline and phenol etc.) are made and various dyes and pigments are then created by combining these intermediates [10]. PAHs compounds are also known to be highly carcinogenic, mutagenic and dioxin-like toxic and their identification is of critical issue since the last years they exhibit noticeable increased concentrations in polluted soil and marine environments [32].

The THz spectra of naphthalene, anthracene, pentacene, phenanthrene (Phen-H), 9-bromo-phenanthrene (Phen-Br) and 9-iodo-phenanthrene (Phen-I) in their crystalline form are shown in Fig. 6. All samples were purchased from Sigma-Aldrich and used without any further purification. In order to avoid scattering losses, the powder samples, before being pressed to pellets (0.5 MPa for 10 minutes), were carefully ground by the aid of a mortar. The thickness of the pellets was ranging between 1.5 and 2.16 mm. As shown in Fig. 6, distinct characteristic absorption peaks can be seen for all the samples. In specific, naphthalene exhibits a resonance peak at 2 THz (67 cm^{-1}) which is in accordance with observations of previous reports [33]. The observed absorption peak is slightly shifted towards lower frequencies in the case of anthracene to 1.84 THz (61 cm^{-1}) and to 1.8 THz (59 cm^{-1}) for phenanthrene. Although the absorption peaks of these three different polyaromatic compounds are located in the frequency range around the 2 THz, the distinction between them is easily seen, since not only the peaks are red-shifted as the number of the aromatic cycles of the compound is increased, but a clear difference on their relative intensity is observed. In case of pentacene, consisting of five linearly fused benzene rings, the THz spectrum becomes more complicated and additional absorption peaks appear at 1.71 THz and around 1 THz.

A remarkable influence on the recorded THz spectra has been observed by replacing a hydrogen atom of a precise position on the aromatic nucleus by halogen atoms. As shown in Fig. 6, the bromination at the 9-position of phenanthrene results to a distinct resonance peak at 1.5 THz (50 cm^{-1}) which is red-shifted to 1.0 THz (33.3 cm^{-1}) if bromium is replaced by the heavier iodide atom. The evident difference in the absorption band position between the two halogenated compounds of phenanthrene is also accompanied by a considerable higher absorbance compared to the resonance peak of the non-halogenated phenanthrene. In order to confirm that the observed resonances are correlated to intermolecular vibrational modes, we performed THz transmission measurements at low temperatures. In Fig. 7 are shown the THz absorption spectra of a 9-iodo-phenanthrene at two different temperatures. One can clearly see that the discrete resonance

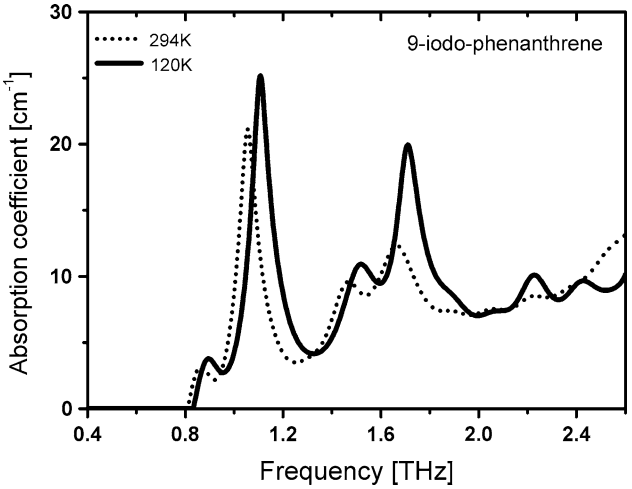

Fig. 7 Absorption spectra of a 9-Iodo-phenanthrene pellet (1.53 mm thick) at two different temperatures

features present at room temperature at 1 THz, 1.46 THz and 1.66 THz become sharper and are shifted towards higher frequencies at lower temperatures. This behavior is associated to the fact that at 294 K the available thermal energy of 25 meV is equivalent to a frequency of 6.12 THz and several vibrational levels are significantly populated. These results in combination with the observation that all absorption peaks disappear completely when the aromatic hydrocarbons are dissolved in solutions provide a clear proof that the observed resonances can be assigned to intermolecular vibrational modes of the microcrystals.

4 Conclusions

In summary we have shown that the use of nonlinear imaging contrast techniques (MPEF, THG) comprise powerful diagnostic tools for art conservation studies since they provide precise in-depth information and the discrimination of the chemical composition of the artifacts. We have also presented the ability of THz imaging in revealing hidden objects as well as the capability of the technique to distinguish strongly absorbing organic compounds like small polycyclic aromatic hydrocarbons and their halogenated compounds. The combination of the above modalities can prove valuable for the non-destructive analysis of different Cultural Heritage related objects and the identification of their composition as a function of depth.

Acknowledgements The authors acknowledge Ms. K. Melessanaki for her expert assistance in the preparation of samples. This work was supported by the EU Marie Curie Excellence Grant "MULTIRAD" MEXT-CT-2006-042683. The EU FP7 Program "LASERLAB-EUROPE" (grant n° 228334) is also acknowledged.

References

1. G. Filippidis, E.J. Gualda, K. Melessanaki, C. Fotakis, Opt. Lett. **33**, 240 (2008)
2. E.J. Gualda, G. Filippidis, K. Melessanaki, C. Fotakis, Appl. Spectrosc. **63**, 280 (2009)
3. P. Vounisiou, A. Selimis, G.J. Tserevelakis, K. Melessanaki, P. Pouli, G. Filippidis, C. Beltsios, S. Georgiou, C. Fotakis, Appl. Phys. A, Mater. Sci. Process. **100**, 647 (2010)
4. P.J. Campagnola, L.M. Loew, Nat. Biotechnol. **21**, 1356 (2003)
5. D. Debarre, E. Beaurepaire, Biophys. J. **92**, 603 (2007)
6. J. Squier, M. Muller, Rev. Sci. Instrum. **72**, 2855 (2001)
7. G. Cormack, P. Losa-Alvarez, L. Sarrado, S. Tomas, I. Amat-Roldan, L. Torner, D. Artigas, J. Guitart, J. Pera, J. Ros, J. Archaeol. Sci. **34**, 1594 (2007)
8. J. Ying, F. Liu, P.P. Ho, R.R. Alfano, Opt. Lett. **25**, 1189 (2000)
9. G. Filippidis, K. Melessanaki, C. Fotakis, Anal. Bioanal. Chem. **395**, 2161 (2009)
10. R.J. Gettens, G.L. Stout, *Painting Materials* (Dover, New York, 1966)
11. A. Nevin, D. Comelli, I. Osticioli, G. Filippidis, K. Melessanaki, G. Valentini, R. Cubeddu, C. Fotakis, Appl. Phys. A, Mater. Sci. Process. **100**, 599 (2010)
12. E. Kendix, G. Moscardi, R. Mazzeo, P. Baraldi, S. Prati, E. Joseph, S. Capelli, J. Raman Spectrosc. **39**, 1104 (2008)
13. A. Nevin, J. Loring Melia, I. Osticioli, G. Gautier, M.P. Colombini, J. Cult. Heritage **9**, 154 (2008)
14. D. Sokara, A.G. Karydas, A. Oikonomou, N. Zacharias, K. Beltsios, V. Kantarelou, Anal. Bioanal. Chem. **395**, 2199 (2009)
15. P. Pouli, A. Selimis, S. Georgiou, C. Fotakis, Acc. Chem. Res. **43**, 771 (2010)
16. E. Kendix, G. Moscardi, R. Mazzeo, P. Baraldi, S. Prati, E. Joseph, S. Capelli, J. Raman Spectrosc. **39**, 1104 (2008)
17. K. Fukunaga, I. Hosako, C. R. Phys. **11**, 519 (2010)
18. J.-M. Manceau, A. Nevin, C. Fotakis, S. Tzortzakis, Appl. Phys. B **90**, 365 (2008)
19. E. Abraham, A. Younus, J.C. Delagnes, P. Mounaix, Appl. Phys. A, Mater. Sci. Process. **100**, 585 (2010)
20. K. Fukunaga, Y. Ogawa, S. Hayashi, I. Hosaka, IEICE Electron. Express **4**, 258 (2007)
21. A.J.L. Adam, P.C.M. Planken, S. Meloni, J. Dik, Opt. Express **17**, 3407 (2009)
22. K. Fukunaga, M. Picollo, Appl. Phys. A, Mater. Sci. Process. **100**, 591 (2010)
23. M. Vanexter, C. Fattinger, D. Grischkowsky, Appl. Phys. Lett. **55**, 337 (1989)
24. X.C. Zhang, Y. Jin, X.F. Ma, Appl. Phys. Lett. **61**, 2764 (1992)
25. H.G. Roskos, M.D. Thomson, M. Kreß, T. Löffler, Laser & Photonics Rev. **1**, 349 (2007)
26. H.D. Wen, A.M. Lindenberg, Phys. Rev. Lett. **103**, 4 (2009)
27. J. Dai, N. Karpowicz, X.C. Zhang, Phys. Rev. Lett. **103**, 023001 (2009)
28. J.-M. Manceau, M. Massaouti, S. Tzortzakis, Opt. Express **18**, 18894 (2010)
29. J.M. Manceau, A. Averchi, F. Bonaretti, D. Faccio, P. Di Trapani, A. Couairon, S. Tzortzakis, Opt. Lett. **34**, 2165 (2009)
30. J.M. Manceau, M. Massaouti, S. Tzortzakis, Opt. Lett. **35**, 2424 (2010)
31. Q. Wu, X.C. Zhang, Appl. Phys. Lett. **68**, 1604 (1996)
32. H.-G. Ni, H. Zeng, S. Tao, E.Y. Zeng, Environ. Toxicol. Chem. **29**, 1237 (2010)
33. J. Han, H. Xu, Z. Zhu, X. Yu, W. Li, Chem. Phys. Lett. **392**, 348 (2004)